Nano-Structures & Nano-Objects 36 (2023) 101063

Contents lists available at ScienceDirect

Nano-Structures & Nano-Objects

journal homepage: www.elsevier.com/locate/nanoso

Fabrication of g-C_3N_4@porphyrin nanorods hybrid material via CTAB surfactant-assisted self-assembly for photocatalytic degradation of Cr(VI) and methylene blue

Quang Dinh Ho [a,1], Tam The Le [a,1], Giang T. Nguyen [b], Du Hoa Nguyen [c], Hao Hoang Nguyen [c], Hiep Thu Thi Le [d], Lam Thanh T. Chu [d], Chinh Van Tran [e], Phuong T. Hoai Nguyen [e], Myoung-Jin Um [f,*], T. Tung Nguyen [b,*], D. Duc Nguyen [f,g], Duong D. La [e,*]

[a] School of Chemistry, Biology and Environment, Vinh University, 182 Le Duan Street, Vinh City, Vietnam
[b] Institute of Materials Science, Vietnam Academy of Science and Technology, 18 Hoang Quoc Viet, Hanoi, Vietnam
[c] Department of Chemistry, College of Education, Vinh University, 182 Le Duan Street, Vinh City, Nghe An Province, Vietnam
[d] Centre for Practice and Experiment, Vinh University, 182 Le Duan Street, Vinh City, Nghe An Province, Vietnam
[e] Institute of Chemistry and Materials, 17 Hoang Sam, Nghia Do, Cau Giay, Hanoi, Vietnam
[f] Department of Civil & Energy System Engineering, Kyonggi University, Suwon, Republic of Korea
[g] Institute of Applied Technology and Sustainable Development, Nguyen Tat Thanh University, Ho Chi Minh City 700000, Vietnam

ARTICLE INFO

Keywords:
Nanorods hybrid material
G-C_3N_4@porphyrin
Self-assembly
Methylene blue removal, photocatalytic degradation

ABSTRACT

Photocatalysts are an attractive solution for pollutant degradation under sunlight irradiation. One approach that has been proposed to enhance their activity is to combine two semiconductors, which can broaden the photon energy harvesting regions and improve charge separation. Herein, a facile approach to fabricating a g-C_3N_4@porphyrin nanorods hybrid material is presented using CTAB surfactant-assisted self-assembly of monomeric porphyrin molecules and g-C3N4 nanomaterials. Using different technical methods, the hybrid material was studied, and it was found that the porphyrin nanorods on the surface of g-C_3N_4 were all in the same place. The photocatalytic performance of the hybrid material was evaluated by investigating its behavior for the photo-oxidation and -degradation of Cr^{6+} ions and methylene blue organic dye under simulated sunlight irradiation. High photocatalytic performance towards these two pollutants was exhibited by the hybrid material with a removal percentage of nearly 100% after 100 min of reaction time under the simulated sunlight spectrum. Also, a possible photocatalytic mechanism of the C_3N_4@porphyrin nanorods photocatalyst was proposed. This mechanism involved the efficient separation and transfer of photo-induced electrons and holes on the surface of the hybrid material. This work offers a simple and efficient method for creating high-performance photocatalysts, and we have made progress in our understanding of their photocatalytic mechanisms. The findings have important implications for wastewater treatment and solar energy conversion. The use of this hybrid material may contribute to addressing environmental challenges and assist in building sustainable energy systems.

1. Introduction

Organic-based supramolecular nanoassemblies are a promising approach for preparing nanostructured materials with controlled morphologies [1–5]. The obtained nanostructured materials reveal unique physicochemical properties, which can be effectively employed in many applications such as sensing, medical and healthcare, photocatalysis, energy storage, and electronic devices [6–11]. Among the methods of organic-based nanomaterials, self-assembly of π-conjugated building block porphyrin derivatives could render the formation of soft solid-state nanomaterials exhibiting interesting light-harvesting properties for photocatalytic reactions, thanks to the low bandgap energy in visible light and capability of mimicking biological processes [12–18]. Many self-assembly strategies have been successfully utilized to prepare π-conjugated porphyrin nanomaterials, including, but not limited to, surfactant-assisted self-assembly, ionic self-assembly, re-precipitation

* Corresponding authors.
E-mail addresses: mum@kyonggi.ac.kr (M.-J. Um), tungnt@ims.vast.ac.vn (T.T. Nguyen), duc.duong.la@gmail.com (D.D. La).
[1] These authors are equally contribution

https://doi.org/10.1016/j.nanoso.2023.101063
Received 18 July 2023; Received in revised form 27 September 2023; Accepted 20 October 2023

self-assembly… [19–23]. The resultant free-standing porphyrin aggregates revealed remarkable photocatalytic activity for the degradation of the organic compound under visible light irradiation [24–28]. Free-standing porphyrin nanostructures such as nanosheets, nanofibers, nanotubes, and microspheres, obtained via self-assembly, revealed highly photocatalytic activity toward organic compounds [27,29]. However, because of fast electron/hole recombination and relatively poor stability, the free-standing porphyrin nanomaterials have been limited for large-scale environmental treatment. To address these problems, the combination with other photocatalysts has been considered a promising solution to improve the absorption of photon energy, and stability, and prevent electron/hole recombination of nanostructured porphyrin, as a result, enhancing the photocatalytic performance of porphyrin-based nanomaterials. Many inorganic semiconductors, such as TiO_2, $CuFe_2O_4$, TiO_2/Fe_2O_3, and graphene, have been successfully incorporated with porphyrin aggregates [30–33]. The resultant porphyrin-based hybrid materials showed enhanced photocatalytic efficiency for the degradation of organic compounds.

An inorganic semiconductor of graphitic carbon nitrides (g-C_3N_4) is intensively applied for pollutant treatment, hydrogen production, sensing, and solar cells, thanks to their high thermal and chemical stabilities and activation with visible light [34–36]. The g-C_3N_4 nanomaterial could be fabricated by sol-gel, mixing, solvothermal, and microwave approaches [37]. Even though free-standing g-C_3N_4 showed that organic compounds in an aqueous solution could be broken down by light, it has not been used in real life because it has a small surface area, does not absorb light well, and loses its charges quickly [38,39]. Like free-standing porphyrin nanomaterials, g-C_3N_4 also needs to incorporate or dope with metals and other semiconductors to improve the surface area, energy harvesting, and charge separation. Many inorganic semiconductors, like $NiSO_4$, TiO_2, $Ca_2Fe_2O_5$, etc., have been successfully mixed with g-C_3N_4 to make hybrid materials, which improved the photocatalytic performance of removing organic compounds by a large amount [40,41]. Notably, most materials with g-C_3N_4 are inorganic semiconductors, and only a few works have been published so far to reveal the integration of g-C_3N_4 with organic semiconductors. Most recently, our group was able to combine g-C_3N_4 with porphyrin nanofiber to make a nanocomposite that was better at removing organic dyes through photocatalysis [42].

Heavy metals have been considered highly toxic substances in water, posing many serious problems for human health and ecosystems [43]. Among them, hexavalent chromium, a carcinogen, and mutagen, are found in many industrial wastewaters such as paper processing, wood processing, paint manufacturing, metal plating, and the leather industry [44,45]. In water, chromium commonly is of two oxidation states trivalent (Cr^{3+}) and hexavalent (Cr^{6+}). It has been well-demonstrated that hexavalent (Cr^{6+}) is extremely hazardous to animal and human lives because of its easy migration through water and soil. In contrast, trivalent chromium (Cr^{3+}) reveals low toxicity to humans due to the formation of $Cr(OH)_3$ precipitation at neutral pH in water [46,47]. Thus, the quest to find an effective way to remove Cr^{6+} from water is urgent to protect the environment and human health.

Herein, this study aims to develop a facile and effective method for fabricating a g-C_3N_4@porphyrin nanorod hybrid material using CTAB surfactant-assisted self-assembly. The combination of nanostructured porphyrin with g-C_3N_4 materials has several advantages such as enhanced photocatalytic performance, increased stability, improved charge separation, and tunable properties. It might contain several disadvantages of high-cost materials, limited long-term stability, and potential agglomeration. The physicochemical properties of the obtained hybrid materials are characterized using various techniques, including UV–vis spectroscopy, scanning electron microscopy (SEM), FTIR, and XRD pattern analysis. The photocatalytic performance of the C_3N_4 @porphyrin nanorods is evaluated for removing Cr^{6+} and methylene blue (MB) under simulated sunlight irradiation, and the proposed photocatalytic mechanism is investigated and discussed to gain a better understanding of the material's photocatalytic activity.

2. Experimental section

2.1. Materials

4,4,4,4-(Porphine-5,10,15,20-tetrayl)tetrakis(benzoic acid) porphyrin was purchased from Shanghai Macklin Biochemical Company. Cetyltrimethylammonium bromide (CTAB) surfactant, methylene blue, $K_2Cr_2O_7$, MB organic dye, sodium hydroxide, hydrochloric acid, urea, and ethanol were obtained from Xilong Chemical Co., Ltd, China. The chemicals were utilized as received and all experiments used double-distilled water as solvent.

2.2. g-C_3N_4 fabrication

Graphitic carbon nitrides were synthesized by the introduction of 10 g urea into a heat-resistant reactor and annealed at a temperature of 550 °C with a reaction time of 3 h. After annealing time, the reactor was cooled down to ambient temperature. The resultant yellow g-C_3N_4 powder thoroughly rose with double-distilled water and ethanol three times each. The purified g-C_3N_4 powder was dried for 5 h at a temperature of 70 °C to obtain g-C_3N_4 nanomaterial and stored at ambient conditions for the next experiment.

2.3. Preparation of g-C_3N_4@porphyrin nanorods hybrid material

g-C_3N_4@porphyrin nanorods were fabricated via *a* CTAB-assisted self-assembly approach of porphyrin monomer and g-C_3N_4 nanomaterial. Typically, 2 mL of NaOH 0.1 M was used to dilute 8 mg of monomeric porphyrin molecule with the addition of 10 mg CTAB surfactant. The g-C_3N_4 was then introduced to the solution with a g-C_3N_4/porphyrin ratio of 3:1 (this ratio was adopted from our previous work) under ultrasonic conditions for 30 min [42]. To induce the self-assembly, 0.1 M of HCl was dropwise to the mixture until the pH solution was in the range of 6–7. The product was centrifuged, rinsed with doubled-distilled water, and thoroughly dried at a temperature of 60 °C overnight. The final product was stored at ambient conditions for further experiments.

2.4. Characterizations

The morphology of the prepared g-C_3N_4@porphyrin hybrid material was observed by scanning electron microscopy (SEM, Hitachi S-4600). The elements composition in the g-C_3N_4@porphyrin was studied by using Energy Dispersive X-ray spectroscopy (EDX, Hitachi S-4600). The UV–vis spectrophotometer (Jasco V730) was used to study the optical properties of the obtained material. The bandgap energy of the g-C_3N_4@porphyrin nanorods semiconductor was determined using the Tauc plot drawn from the UV–vis diffuse reflectance spectrum. The photocatalytic experiment was also studied using a UV–vis spectrophotometer.

2.5. Photocatalytic activity testing

The simulated sunlight testing chamber was fabricated using a xenon lamp 350 W as a light source with water surrounding the jet for cooling down the reaction chamber. For the Cr^{6+} photocatalytic removal experiment, 0.4 mg of the photocatalyst was added to the 20 mL of Cr^{6+} solution with a concentration of 20 ppm. Before placing it into the reaction chamber, the adsorption equilibrium of the mixture was established in dark conditions overnight. After introducing it to the simulated sunlight chamber, at specific time intervals, 3 mL of the mixture was withdrawn, and its UV–vis spectrum was measured. The Cr^{6+} removal percentage was determined by monitoring the change in absorption peaks at the wavelength of 373 nm. Another experiment was conducted

to examine the photocatalytic efficiency of the g-C_3N_4@porphyrin nanorods photocatalyst in the photodegradation of MB with a concentration of 10 ppm recorded at the wavelength of 662 nm.

3. Results and discussion

Illustrated in Fig. 2 are the SEM images of, free-standing g-C_3N_4, and porphyrin aggregates. The g-C_3N_4@porphyrin nanorods were prepared with CTAB-assisted self-assembly at the g-C_3N_4/porphyrin ratio of 3:1. The nanosheet shape of free-standing g-C_3N_4 is observed in Fig. 1a with a diameter on the microscale and thickness on the nanoscale. The porphyrin aggregates without the presence of g-C_3N_4 reveal a rod-like structure with a diameter of around 50 nm and a length in a range of 200–500 nm (Fig. 1b). After the CTAB-assisted self-assembly process of porphyrin monomer with the presence of g-C_3N_4, well-defined porphyrin nanorods were uniformly observed on the surface of g-C_3N_4, indicating the successful formation of g-C_3N_4@porphyrin nanorod materials.

The elemental composition of the material was investigated by Energy-dispersive X-ray spectroscopy. Fig. 2 shows the EDS spectra of free-standing g-C_3N_4 and g-C_3N_4@porphyrin nanorods nanocomposite prepared via CTAB-assisted self-assembly at the g-C_3N_4/porphyrin ratio of 3:1. The elemental analysis showed that the atomic percentages of C and N in g-C3N4 were 36.92% and 63.08%, respectively, this is consistent with the expected stoichiometric ratio of C and N in the g-C_3N_4 compound [48]. After self-assembly with porphyrin molecules, the atomic percentage of N decreased to 46.82% and the atomic percentage of C increased to 43.21%. The O element was also observed in the EDS spectrum of g-C_3N_4@porphyrin nanorod hybrid material with an atomic percentage of 8.9%. This change in the atomic percentages is ascribed to the presence of N, C, and O elements from the porphyrin molecules, demonstrating the successful integration of g-C_3N_4 and porphyrin nanorods to form hybrid material.

Illustrated in Fig. 3 are the UV–vis spectra of porphyrin monomers and g-C_3N_4@porphyrin nanorods prepared at the g-C_3N_4/porphyrin ratio of 3:1 to investigate the optical properties of the material. It has been well-perceived that the porphyrin monomer's UV–vis spectrum consists of two bands named the Soret band and Q-absorption bands (in the range of 500–700 nm). While the Soret band is formed by the $a_{1u}(\pi)$ to $e^*_g(\pi)$ transition, the presence of Q-absorption bands is due to the transition of the $a_{2u}(\pi)$ to $e^*_g(\pi)$ transition in porphyrin molecules [49,50]. In this work, these two bands were also observed at 411 nm (Soret band) and 04 weak Q absorption bands (in the range of 500–700 nm) in the UV–vis spectrum of the porphyrin molecule as can be seen in Fig. 3 (black line). The UV–vis spectrum of the g-C_3N_4@porphyrin nanorods nanocomposite exhibited a broad absorption peak at 417 nm, which belonged to the Soret band with significantly low intensity in comparison to that of monomeric porphyrin molecule, indicating the aggregate phenomenon of the porphyrin monomer. The UV–vis spectra of the porphyrin monomer and aggregates displayed a red shift in the Soret band, from 411 nm to 420 nm, respectively, indicating the distinct bathochromic and hypsochromic shift of *J*-type aggregates induced by the self-assembly process of monomeric porphyrin molecules [21,51,52]. The *J*-type aggregates were also evident by the integration of four weak peaks in Q bands of porphyrin monomer into one broadband at 671 nm in porphyrin aggregates. This result demonstrates that the porphyrin monomer has successfully assembled into nanostructures on the surface of g-C_3N_4 nanomaterials, which is observed in the SEM image above.

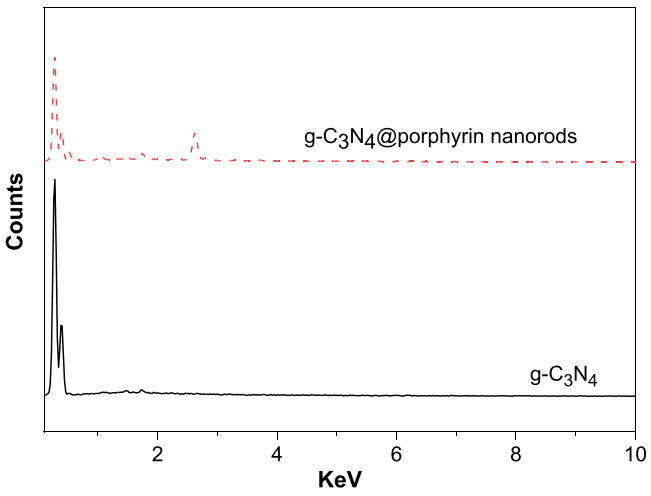

Fig. 2. EDS spectra of free-standing g-C_3N_4 and g-C_3N_4@porphyrin nanorods nanocomposite prepared via CTAB-assisted self-assembly at the g-C_3N_4/porphyrin ratio of 3:1.

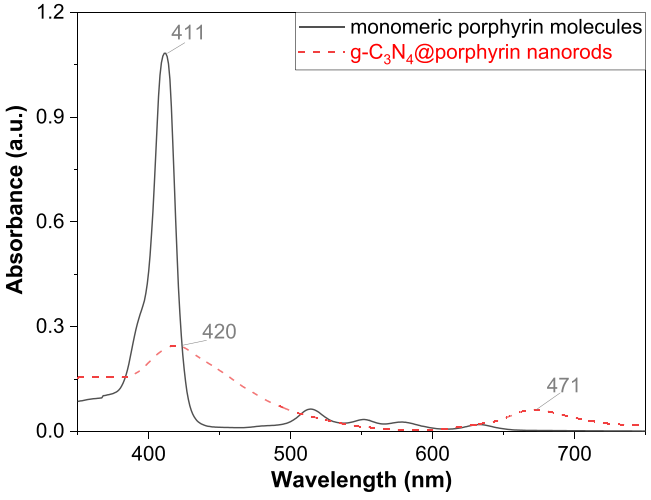

Fig. 3. UV–vis spectra of porphyrin monomer and g-C_3N_4@porphyrin nanorods prepared at the g-C_3N_4/porphyrin ratio of 3:1.

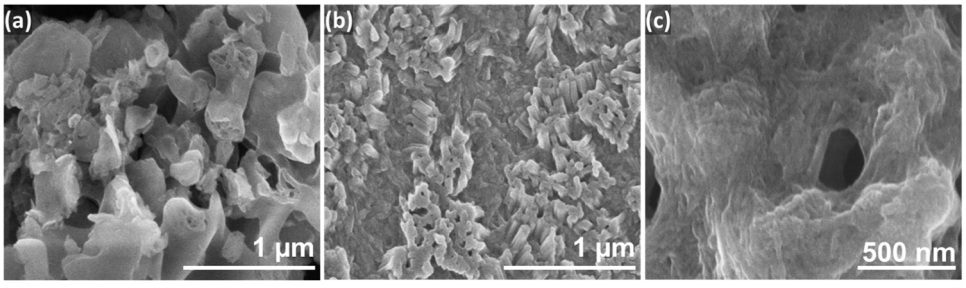

Fig. 1. The SEM images of (a) free-standing g-C_3N_4 nanomaterial, (b) free-standing porphyrin aggregates, and (c) g-C_3N_4 @porphyrin nanorods prepared via CTAB-assisted self-assembly at the g-C_3N_4/porphyrin ratio of 3:1.

The crystallinity properties of the g-C_3N_4@porphyrin nanorods fabricated at the g-C_3N_4/porphyrin ratio of 3:1 were investigated by X-ray diffraction (XRD) technique and the result is exhibited in Fig. 4. In the XRD pattern, the diffraction peak at around 12.8 and 28° is ascribed to the (100) and (002) planes, respectively, of the g-C_3N_4 nanomaterials (JCPDS No. 87–1526) [53–55]. While the (002) plane is formed by the aromatic layers stacking, the stacking of tri-s-triazine units in the g-C_3N_4 is responsible for the formation of the (100) plane. These diffraction peaks of g-C_3N_4 nanomaterial reveal a small shift compared to the pristine g-C_3N_4 demonstrating the electronic interaction between g-C_3N_4 and porphyrin aggregates. Furthermore, the XRD pattern of the hybrid material also appears strong peaks at approximately 32, 33, 45, and 47°, which are assumed as diffraction peaks of the nanostructured porphyrin, indicating that the self-assembled porphyrin is of high crystalline in nature as well as well-defined crystallinity of the resultant g-C_3N_4@porphyrin nanorods nanocomposite.

The Fourier transform infrared technique was employed to investigate the chemical bonding in the material. The FTIR spectrum of the produced material showed a vibrational band at around 3249 cm^{-1}, which can be attributed to the –COOH and –OH groups of the porphyrin molecules and moisture absorbed on the hybrid material (Fig. 5). The C═O and C-O sketching vibration modes in the carbonyl groups of the porphyrin monomer are also observed in the FTIR spectrum with the appearance of absorption peaks at 1625 and 1396 cm^{-1}, respectively [56]. The absorption bands at 1312 and 1227 cm^{-1} are ascribed to the presence of the C-NH-C bridge and C-N(-C), respectively, in g-C_3N_4 material [57]. The other firm peaks presented in the range of 1950 – 1630 cm^{-1} of the FTIR spectrum are assigned to the sketching vibrations of heptazine-derived repeating units and C-N heterocycles of the g-C $_3N_4$ [58]. The absorption bands at around 820 and 707 cm^{-1} are the characteristic sketching of tri-s-triazine modes. This result provides further evidence of the successful formation of the well-integrated g-C_3N_4@porphyrin nanomaterial.

The bandgap energy of the g-C_3N_4@porphyrin nanorods nanocomposite was determined using the Tauc plot drawn from the diffuse reflectance UV–vis spectrum, as exhibited in Fig. 6. The Tauc plot indicates that the hybrid material has two bandgap energies of 2.3 and 2.64 eV, making it capable of absorbing photon energy within the visible light spectrum. The results suggest that the prepared hybrid material has potential as a novel photocatalyst that can activate in the visible light region for environmental treatment purposes.

It has been well-known that the molecular structure of porphyrin aggregates are similar to the photoactive molecules, which are responsible for the many biological photo-transduction processes in ecosystems

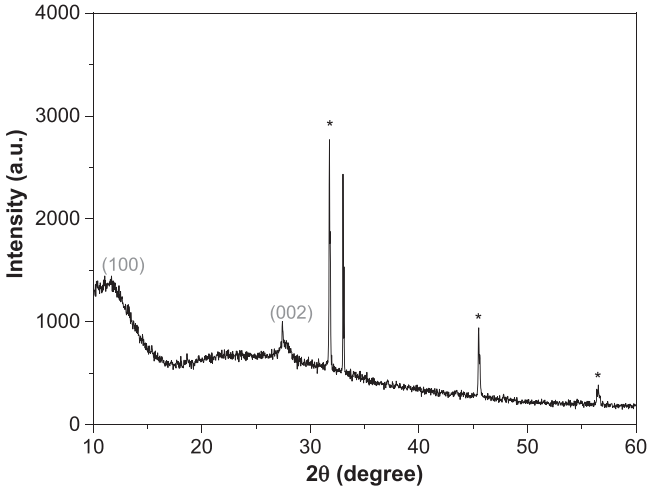

Fig. 4. XRD pattern of g-C_3N_4@porphyrin nanorods prepared at the g-C_3N_4/porphyrin ratio of 3:1.

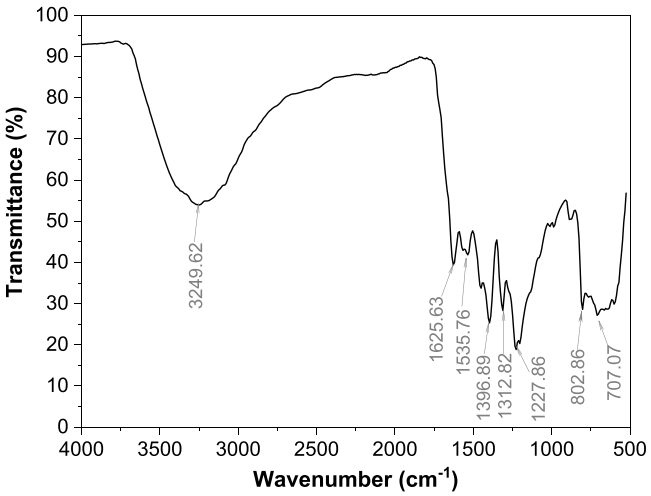

Fig. 5. FTIR spectrum of g-C_3N_4@porphyrin nanorods prepared at the g-C_3N_4/porphyrin ratio of 3:1.

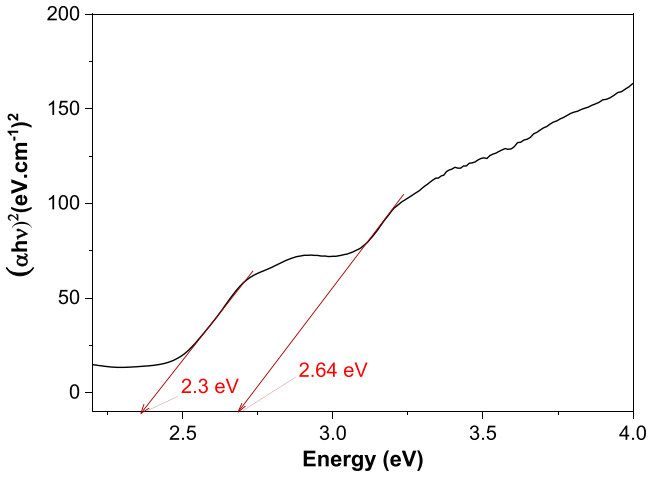

Fig. 6. The Tauc plot of g-C_3N_4@porphyrin nanorods hybrid material prepared at the g-C_3N_4/porphyrin ratio of 3:1.

[59,60]. Among the photocatalytic activity of the porphyrin nanostructures, porphyrin nanorods seem to have higher photocatalytic performance compared to the nanostructured porphyrin with other morphologies reported previously [61]. The g-C_3N_4 nanomaterials have been reported to have highly photocatalytic activity in the near-UV and visible light region because of their low bandgap energies ranging from 2 to 3 eV [62,63]. The formation of hybrid material resulted in two bandgap energies (2.3 and 2.64 eV), suggesting that the material could serve as an efficient photocatalyst across a broad range of the light spectrum. The formation of an interface junction between g-C_3N_4 and porphyrin nanorods could significantly suppress the charge recombination; as a result, enhancing the photocatalytic performance. To test this hypothesis, we conducted a photocatalytic experiment using g-C_3N_4@porphyrin nanorods as the photocatalysts to degrade Cr^{6+} ions and MB under simulated sunlight irradiation. The photocatalytic activity of the prepared photocatalyst for the removal of Cr^{6+} ions under simulated sunlight irradiation is depicted in Fig. 7. As illustrated in Fig. 7a, the Cr^{6+} concentration noticeably decreases upon exposure to the sunlight spectrum in the presence of the photocatalysts. The Cr^{6+} was observed to be removed from the aqueous solution after 30 min of the reaction time. This evidence is seen in Fig. 7b with more than 50% of Cr^{6+} degraded only after 10 min and nearly 96% of Cr^{6+} was removed from the aqueous solution was removed after 30 min of reaction time.

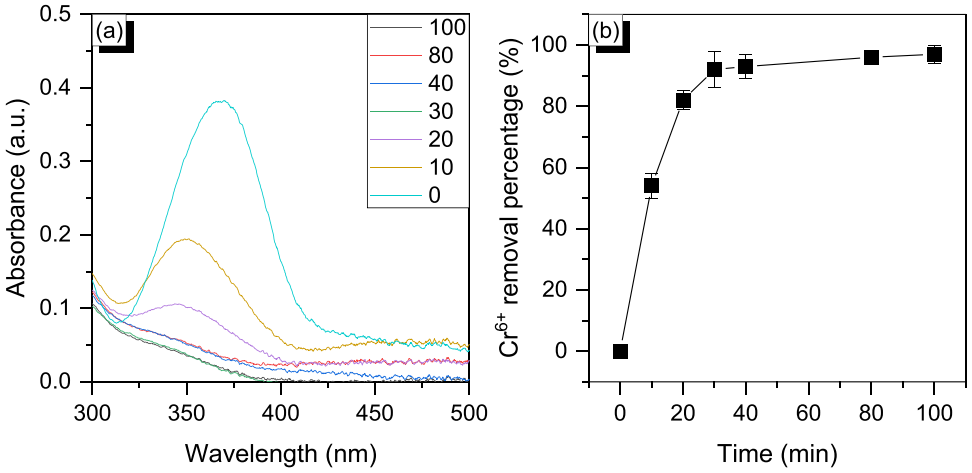

Fig. 7. (a) UV-spectra of Cr^{6+} in aqueous solution and (b) Cr^{6+} removal percentage at various photocatalytic reaction times by g-C_3N_4@porphyrin nanorods photocatalyst under irradiation of simulated sunlight.

The Cr^{6+} was witnessed to be entirely removed from the aqueous solution after 80 min of light irradiation. This result indicates that the g-C_3N_4@porphyrin nanorods could be utilized as a highly effective photocatalyst for the removal of toxic Cr^{6+} in an aqueous solution only using photon energy from sunlight.

Fig. 8 displays the study of the photodegradation of MB by the g-C_3N_4@porphyrin nanorods photocatalyst prepared under simulated sunlight irradiation. In the absence of photocatalyst condition, virtually no MB degradation is observed even after 100 min of light irradiating. However, when g-C_3N_4@porphyrin nanorods photocatalyst was introduced, the MB dyes were degraded quickly and reached nearly 100% MB removal after 100 min of reaction time. These findings provide further confirmation of the exceptional photocatalytic activity exhibited by the photocatalyst hybrid material prepared when activated by simulated sunlight irradiation.

Three kinetic models of photo-degradation of Cr(VI) and MB were studied. The investigated models are followed by Eqs. (1), (2), and (3) for the linear forms of the zero-, first-, and second-order kinetic models, respectively.

$$C_t = C_0 - k_0 t \tag{1}$$

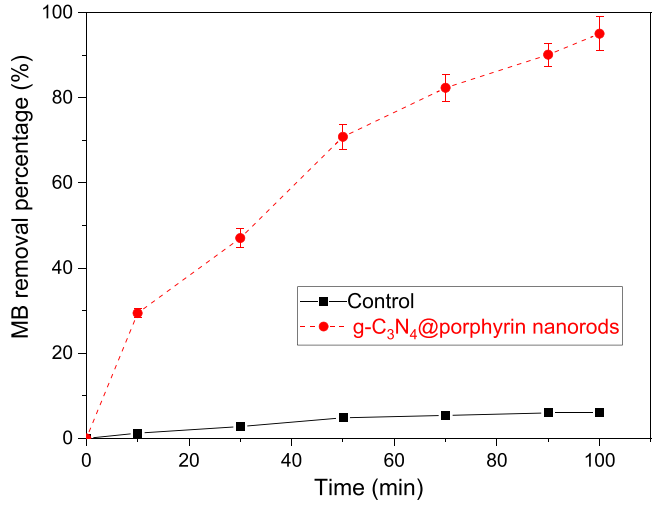

Fig. 8. Methylene blue (MB) removal percentage at various photocatalytic reaction time by g-C_3N_4@porphyrin nanorods under simulated irradiation of sunlight.

$$\ln \frac{C_t}{C_0} = -k_1 t \tag{2}$$

$$\frac{1}{C_t} = \frac{1}{C_0} + k_2 t \tag{3}$$

Where, C_0, C_t are the initial concentrations and the concentrations at reaction time t (mg/L) of the pollutants solution; k_0, k_1, and k_2 are the constant rates of the zero-, first- and second-order kinetic models, respectively. The results are presented in Fig. 9 and Fig. 10. The kinetic parameters of zero-order, first-order, and second-order models for the degradation of Cr(VI), and MB are mentioned in Table 1.

Comparing the regression coefficients (R^2) obtained in Table 1, it can be seen that the kinetic degradation of Cr(VI) is well-fitted by the second-order model, while the kinetic degradation of MB solution is well fitted by the first-order model. The apparent kinetic rate constant, k_2, k_1, of the degradation of Cr(VI), and MB solution were found to be 0.0162 L/mg.min, and 0.0279 min^{-1}, respectively.

The recyclability of the g-C_3N_4@porphyrin nanorods was investigated for the photodegradation of Cr(VI) and MB upto 5 cycles. After each cycle, the catalyst was centrifuged, rinsed thoroughly with double distilled water, dried completely before use for the next cycle. The results are shown in Fig. 11. It is obvious that the removal percentages of the MB and Cr(VI) decrease negatively after 5 cycles of testing, demonstrating that the g-C_3N_4@porphyrin nanorods photocatalyst is relatively stable in the aqueous solution. The XRD pattern of the spent photocatalyst was obtained and shown in Fig. S1. The diffraction peaks appear in the XRD pattern of the spent catalyst are similar to that of the pristine g-C_3N_4@porphyrin nanorods before the photodegradation process. This result further confirms the stability of the catalyst for the photodegradation of the MB and Cr(VI) in aqueous solution.

The photo-semiconductor property of J-type porphyrin aggregates' π-conjugate arises from the rigid π-π intermolecular interactions within the porphyrin's core [33]. The photo-semiconductor property means that there exists a bandgap energy in the molecular structure of porphyrin aggregates, which enables the material to absorb photon energy and generate electron/hole pairs for the photocatalytic reaction [52,56,64]. Because of the interface junction between g-C_3N_4 and porphyrin nanorods, the photon-induced charge could transfer between these two semiconductors to prevent the electrons and holes recombination; as a result, enhancing the photocatalytic performance [65,66]. The g-C_3N_4@porphyrin nanorods possess two bandgap energies (2.3 and 2.64 eV), allowing them to effectively harvest photon energy across a broad range of the solar spectrum, particularly in the visible region. Based on these results and established knowledge, we propose and

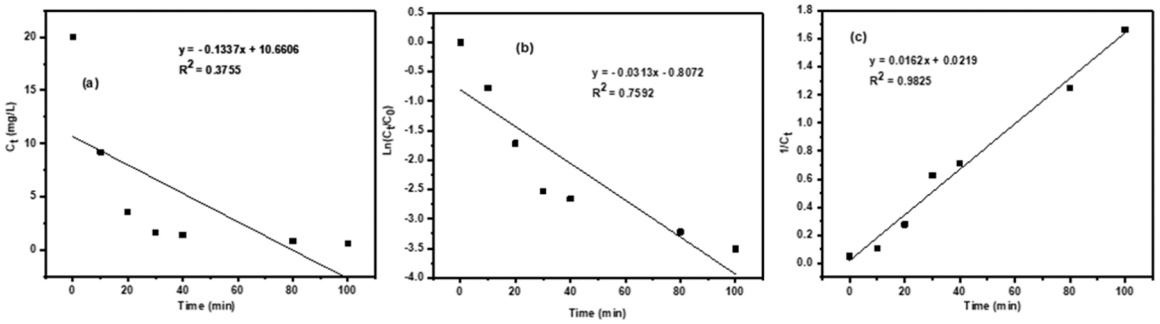

Fig. 9. Fitting of Cr(VI) degradation data with the (a) zero-, (b) first-, and (c) second-order kinetic model.

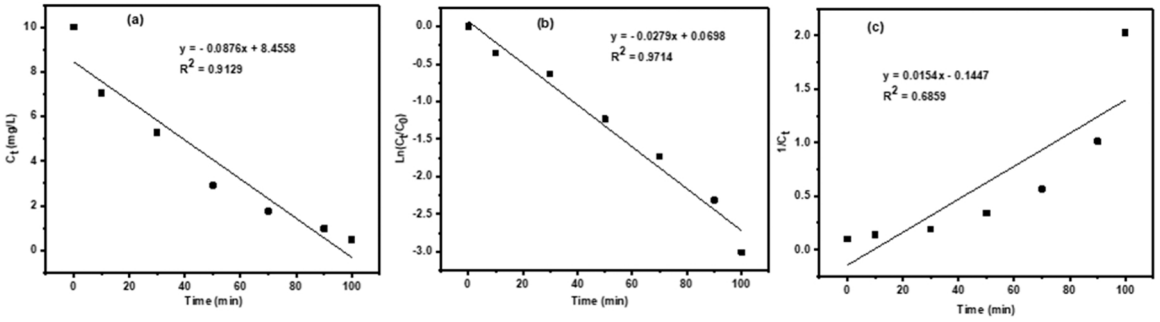

Fig. 10. Fitting of MB degradation data with the (a) zero-, (b) first-, and (c) second-order kinetic model.

discuss a potential mechanism for the improved photocatalytic performance of the nanorods photocatalyst prepared in degrading Cr^{6+} and MB. In the first stage after irradiating with the sunlight, electrons in the valence band of the porphyrin nanorods and g-C_3N_4 absorb enough energy from the photon to jump to the conduction band and left holes in the valence band [27]. The newly generated electrons in the conduction bands will move from g-C_3N_4 to porphyrin nanorods and in the reverse direction, the holes will diffuse through the interface from porphyrin nanorods to g-C_3N_4. These exciton-coupled charge transfer processes significantly suppress the recombination of photon-induced electron/-hole pairs. This, in turn, allows for greater participation of electrons and holes in the photocatalytic reaction. For the Cr^{6+} degradation, the newly generated electrons could directly reduce highly toxic Cr^{6+} to less toxic Cr^{3+}. For the MB photodegradation, free radicals such as $^{\bullet}O_2^-$, $OH^{\bullet}$. generated from the reduction reaction between electrons and O_2 and/or H_2O will oxidize MB to less harmful substances; and the holes could also directly oxidize MB dyes to less toxic compounds.

4. Conclusion

In short, the g-C_3N_4@porphyrin nanorods hybrid material has been successfully fabricated via CTAB-assisted self-assembly of porphyrin monomers and g-C_3N_4 nanomaterials at the g-C_3N_4/porphyrin ratio of 3:1. The prepared hybrid material demonstrated excellent integration between the porphyrin nanorods, which had a diameter of

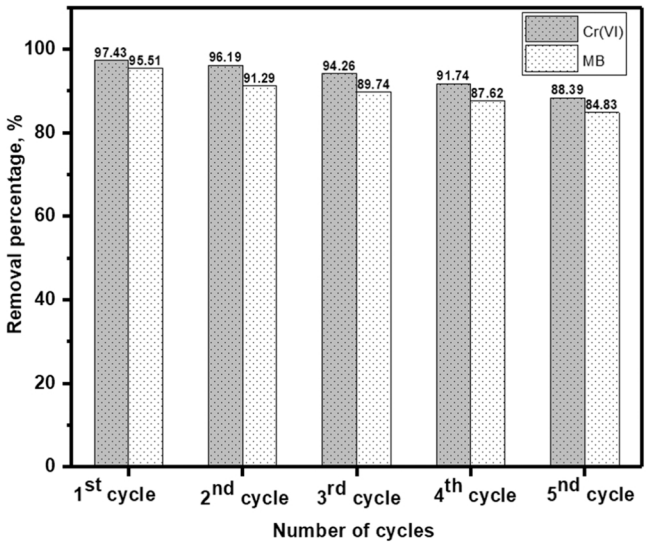

Fig. 11. The reusability of g-C_3N_4@porphyrin nanorods for Cr(VI) and MB degradation for five cylces.

Table 1
Parameters of the zero-,first-, and second-order kinetic models for pollutant degradation.

Kinetic models	Parameters	For Cr (VI) degradation	For MB degradation
Zero-order kinetic model	k_0 (mg/L.min)	0.1337	0.0876
	R^2	0.3755	0.9129
First-order kinetic model	k_1 (min^{-1})	0.0313	0.0279
	R^2	0.7592	0.9714
Second-order kinetic model	k_2 (L/mg.min)	0.0162	0.0154
	R^2	0.9825	0.6859

approximately 50 nm and a length ranging from 200 to 500 nm. The resulting g-C3N4@porphyrin nanorods exhibit two bandgap energies of 2.3 and 2.64 eV, enabling them to absorb photon energy across a wide range of the solar spectrum, particularly in the visible light region. When used as the photocatalyst, the hybrid material revealed quick and highly effective photodegradation of Cr^{6+} ion in an aqueous solution with more than 95% removal percentage only after 30 min of reaction time under simulated sunlight irradiation. The g-C_3N_4@porphyrin nanorods also exhibited remarkably photocatalytic behavior toward methylene blue with a removal percentage of 100% after 100 min of irradiating time. The superior photocatalytic performance of the resulting hybrid material can be attributed to its efficient photon-energy harvesting and enhanced charge separation, which is achieved through exciton-coupled charge transfer processes at the interfaces of the two semiconductors. The high photocatalytic activity exhibited by the g-C_3N_4@porphyrin nanorods suggests their potential as a promising photocatalyst for the removal of pollutants from wastewater.

CRediT authorship contribution statement

Quang Dinh Ho: Conceptualization, Investigation, Writing – original draft. **Tam The Le:** Conceptualization, Investigation, Writing – original draft. **Giang T. Nguyen:** Formal analysis, Writing – original draft. **Du Hoa Nguyen:** Methodology, Writing – review & editing, Resources. **Hao Hoang Nguyen:** Conceptualization, Methodology, Investigation. **Hiep Thu Thi Le:** Investigation, Writing – original draft. **Lam Thanh T. Chu:** Writing – review & editing. **Chinh Van Tran:** Resources, Writing – review & editing. **Phuong T. Hoai Nguyen:** Resources, Writing – review & editing. **Myoung-Jin Um:** Resources, Funding acquisition. **T. Tung Nguyen:** Methodology, Funding acquisition, Writing – review & editing, Resources. **D. Duc Nguyen:** Supervision, Funding acquisition, Writing – review & editing, Resources. **Duong D. La:** Methodology, Funding acquisition, Writing – review & editing, Resources.

Declaration of Competing Interest

The authors declare that they have no known competing financial interests or personal relationships that could have appeared to influence the work reported in this paper.

Data availability

Data will be made available on request.

Acknowledgment

This research was financially supported by the Ministry of Education and Training (MOET) under Project No. B2023-TDV-04.

Appendix A. Supporting information

Supplementary data associated with this article can be found in the online version at doi:10.1016/j.nanoso.2023.101063.

References

[1] S. Park, J.-H. Lim, S.-W. Chung, C.A. Mirkin, Self-assembly of mesoscopic metal-polymer amphiphiles, Science 303 (5656) (2004) 348–351.
[2] E. Winfree, F. Liu, L.A. Wenzler, N.C. Seeman, Design and self-assembly of two-dimensional DNA crystals, Nature 394 (6693) (1998) 539–544.
[3] M. Byun, W. Han, B. Li, X. Xin, Z. Lin, An unconventional route to hierarchically ordered block copolymers on a gradient patterned surface through controlled evaporative self-assembly, Angew. Chem. Int. Ed. 52 (4) (2013) 1122–1127.
[4] P.C. Ray, Size and shape-dependent second order nonlinear optical properties of nanomaterials and their application in biological and chemical sensing, Chem. Rev. 110 (9) (2010) 5332–5365.
[5] S. Kaviya, Synthesis, self-assembly, sensing methods and mechanism of bio-source facilitated nanomaterials: a review with future outlook, Nano-Struct. Nano-Objects 23 (2020), 100498.
[6] J. Xiao, L. Qi, Surfactant-assisted, shape-controlled synthesis of gold nanocrystals, Nanoscale 3 (4) (2011) 1383–1396.
[7] J. Jang, J.H. Oh, Facile fabrication of photochromic dye–conducting polymer core–shell nanomaterials and their photoluminescence, Adv. Mater. 15 (12) (2003) 977–980.
[8] S. Ramezanpour, I. Sheikhshoaie, M. Khatamian, Constructing Mn3O4/Cu hybrid nanorods as superior photocatalyst, Nano-Struct. Nano-Objects 16 (2018) 396–402.
[9] S. Jain, A.P. Shah, N.G. Shimpi, An efficient photocatalytic degradation of organic dyes under visible light using zinc stannate (Zn2SnO4) nanorods prepared by microwave irradiation, Nano-Struct. Nano-Objects 21 (2020), 100410.
[10] M.H. Ahmadi, M. Ghazvini, M. Sadeghzadeh, M.A. Nazari, M. Ghalandari, Utilization of hybrid nanofluids in solar energy applications: a review, Nano-Struct. Nano-Objects 20 (2019), 100386.
[11] A. Shourya, H.P. Dasari, Formation of nano-rod structures in manganese-rich ceria–manganese mixed oxides and their soot oxidation activity, Nano-Struct. Nano-Objects 34 (2023), 100970.
[12] K. Sakakibara, J.P. Hill, K. Ariga, Thin-film-based nanoarchitectures for soft matter: controlled assemblies into two-dimensional worlds, Small 7 (10) (2011) 1288–1308.
[13] F. Würthner, T.E. Kaiser, C.R. Saha-Möller, J-Aggregates: from serendipitous discovery to supramolecular engineering of functional dye materials, Angew. Chem. Int. Ed. 50 (15) (2011) 3376–3410.
[14] C. Zhang, P. Chen, H. Dong, Y. Zhen, M. Liu, W. Hu, Porphyrin supramolecular 1D structures via surfactant-assisted self-assembly, Adv. Mater. 27 (36) (2015) 5379–5387.
[15] C.M. Drain, A. Varotto, I. Radivojevic, Self-organized porphyrinic materials, Chem. Rev. 109 (5) (2009) 1630–1658.
[16] J.A. Elemans, R. van Hameren, R.J. Nolte, A.E. Rowan, Molecular materials by self-assembly of porphyrins, phthalocyanines, and perylenes, Adv. Mater. 18 (10) (2006) 1251–1266.
[17] F.J. Hoeben, P. Jonkheijm, E. Meijer, A.P. Schenning, About supramolecular assemblies of π-conjugated systems, Chem. Rev. 105 (4) (2005) 1491–1546.
[18] D. Lee, K.-D. Kim, Y.-K. Lee, Conversion of V-porphyrin in asphaltenes into V2S3 as an active catalyst for slurry phase hydrocracking of vacuum residue, Fuel 263 (2020), 116620.
[19] S.J. Lee, J.T. Hupp, S.T. Nguyen, Growth of narrowly dispersed porphyrin nanowires and their hierarchical assembly into macroscopic columns, J. Am. Chem. Soc. 130 (30) (2008) 9632–9633.
[20] S.J. Lee, C.D. Malliakas, M.G. Kanatzidis, J.T. Hupp, S.T. Nguyen, Amphiphilic porphyrin nanocrystals: morphology tuning and hierarchical assembly, Adv. Mater. 20 (18) (2008) 3543–3549.
[21] P. Guo, P. Chen, W. Ma, M. Liu, Morphology-dependent supramolecular photocatalytic performance of porphyrin nanoassemblies: from molecule to artificial supramolecular nanoantenna, J. Mater. Chem. 22 (38) (2012) 20243–20249.
[22] Z. Wang, C.J. Medforth, J.A. Shelnutt, Porphyrin nanotubes by ionic self-assembly, J. Am. Chem. Soc. 126 (49) (2004) 15954–15955.
[23] E. Harputlu, K. Ocakoglu, F. Yakuphanoglu, A. Tarnowska, D.T. Gryko, Physical properties of self-assembled zinc chlorin nanowires for artificial light-harvesting materials, Nano-Struct. Nano-Objects 10 (2017) 9–14.
[24] La, D.D. Porphyrin-based nanomaterials and their applications for photocatalysis. RMIT University, 2017.
[25] D.D. La, R.W. Jadha, N.M. Gosavi, E.R. Rene, T.A. Nguyen, B. Xuan-Thanh, D. D. Nguyen, W.J. Chung, S.W. Chang, X.H. Nguyen, Nature-inspired organic semiconductor via solvophobic self-assembly of porphyrin derivative as an effective photocatalyst for degradation of rhodamine B dye, J. Water Process Eng. 40 (2021), 101876.
[26] D.D. La, T.D. Dang, P.C. Le, X.T. Bui, S.W. Chang, W.J. Chung, S.C. Kim, D. D. Nguyen, Self-assembly of monomeric porphyrin molecules into nanostructures: self-assembly pathways and applications for sensing and environmental treatment, Environ. Technol. Innov. (2023), 103019.
[27] D.D. La, H.H. Ngo, D.D. Nguyen, N.T. Tran, H.T. Vo, X.H. Nguyen, S.W. Chang, W. J. Chung, M.D.-B. Nguyen, Advances and prospects of porphyrin-based nanomaterials via self-assembly for photocatalytic applications in environmental treatment, Coord. Chem. Rev. 463 (2022), 214543.
[28] R.W. Jadhav, D.D. La, T.N. Truong, S.V. Khalap, D.V. Quang, S.V. Bhosale, The controllable nanostructure and photocatalytic behaviour of 5, 10, 15, 20-tetra-(3, 4, 5 trimethoxyphenyl) porphyrin through solvophobic supramolecular self-assembly, New J. Chem. 44 (42) (2020) 18442–18448.
[29] Y. Zhong, Z. Wang, R. Zhang, F. Bai, H. Wu, R. Haddad, H. Fan, Interfacial self-assembly driven formation of hierarchically structured nanocrystals with photocatalytic activity, ACS Nano 8 (1) (2014) 827–833.
[30] D. La, R. Hangarge, S. V Bhosale, H. Ninh, L. Jones, S. Bhosale, Arginine-mediated self-assembly of porphyrin on graphene: a photocatalyst for degradation of dyes, Appl. Sci. 7 (6) (2017) 643.
[31] D.D. La, S.V. Bhosale, L.A. Jones, S.V. Bhosale, Arginine-induced porphyrin-based self-assembled nanostructures for photocatalytic applications under simulated sunlight irradiation, Photochem. Photobiol. Sci. 16 (2) (2017) 151–154.
[32] D.D. La, A. Rananaware, M. Salimimarand, S.V. Bhosale, Well–dispersed assembled porphyrin nanorods on graphene for the enhanced photocatalytic performance, ChemistrySelect 1 (15) (2016) 4430–4434.

[33] M.D. Aljabri, D.D. La, R.W. Jadhav, L.A. Jones, D.D. Nguyen, S.W. Chang, L. Dai Tran, S.V. Bhosale, Supramolecular nanomaterials with photocatalytic activity obtained via self-assembly of a fluorinated porphyrin derivative, Fuel 254 (2019), 115639.
[34] J. Safaei, N.A. Mohamed, M.F.M. Noh, M.F. Soh, N.A. Ludin, M.A. Ibrahim, W.N.R. W. Isahak, M.A.M. Teridi, Graphitic carbon nitride (gC 3 N 4) electrodes for energy conversion and storage: a review on photoelectrochemical water splitting, solar cells and supercapacitors, J. Mater. Chem. A 6 (45) (2018) 22346–22380.
[35] Z. Huang, X. Zeng, K. Li, S. Gao, Q. Wang, J. Lu, Z-scheme NiTiO3/g-C3N4 heterojunctions with enhanced photoelectrochemical and photocatalytic performances under visible LED light irradiation, ACS Appl. Mater. Interfaces 9 (47) (2017) 41120–41125.
[36] R. Malik, V.K. Tomer, V. Chaudhary, M.S. Dahiya, A. Sharma, S. Nehra, S. Duhan, K. Kailasam, An excellent humidity sensor based on In–SnO 2 loaded mesoporous graphitic carbon nitride, J. Mater. Chem. A 5 (27) (2017) 14134–14143.
[37] M. Ahmaruzzaman, S.R. Mishra, Photocatalytic performance of g-C3N4 based nanocomposites for effective degradation/removal of dyes from water and wastewater, Mater. Res. Bull. 143 (2021), 111417.
[38] D. Mohanta, A. Mahanta, S.R. Mishra, S. Jasimuddin, M. Ahmaruzzaman, Novel SnO2@ ZIF-8/gC3N4 nanohybrids for excellent electrochemical performance towards sensing of p-nitrophenol, Environ. Res. 197 (2021), 111077.
[39] T. Muhmood, M.A. Khan, M. Xia, W. Lei, F. Wang, Y. Ouyang, Enhanced photo-electrochemical, photo-degradation and charge separation ability of graphitic carbon nitride (g-C3N4) by self-type metal free heterojunction formation for antibiotic degradation, J. Photochem. Photobiol. A: Chem. 348 (2017) 118–124.
[40] S. Yang, Q. Sun, W. Han, Y. Shen, Z. Ni, S. Zhang, L. Chen, L. Zhang, J. Cao, H. Zheng, A simple and highly efficient composite based on gC 3 N 4 for super rapid removal of multiple organic dyes from water under sunlight, Catal. Sci. Technol. 12 (3) (2022) 786–798.
[41] D.S. Vavilapalli, R.G. Peri, R. Sharma, U. Goutam, B. Muthuraaman, R. Rao, S. Singh, g-C3N4/Ca2Fe2O5 heterostructures for enhanced photocatalytic degradation of organic effluents under sunlight, Sci. Rep. 11 (1) (2021) 1–11.
[42] H.T. Lai, G.T. Nguyen, N.T. Tran, T.T. Nguyen, C. Van Tran, D.K. Nguyen, S. Chang, W.J. Chung, D.D. Nguyen, H.P.N. Thi, Assembled porphyrin nanofiber on the surface of g-C3N4 nanomaterials for enhanced photocatalytic degradation of organic dyes, Catalysts 12 (12) (2022) 1630.
[43] H. Hu, Human health and heavy metals, Life Support.: Environ. Hum. Health (2002) 65.
[44] N. Spanos, S. Slavov, C. Kordulis, A. Lycourghiotis, Mechanistic aspects of the deposition of the Cr (VI) species on the surface of TiO2 and SiO2, Coll. Surf. A Physicochem. Eng. Asp. 97 (2) (1995) 109–117.
[45] P.R. Wittbrodt, C.D. Palmer, Reduction of Cr (VI) in the presence of excess soil fulvic acid, Environ. Sci. Technol. 29 (1) (1995) 255–263.
[46] S. Feng, J. Ni, S. Li, X. Cao, J. Gao, W. Zhang, F. Chen, R. Huang, Y. Zhang, S. Feng, Removal of hexavalent chromium by electrospun silicon dioxide nanofibers embedded with copper-based organic frameworks, Sustainability 14 (21) (2022) 13780.
[47] S. Georgios, L. Lefteris, M. Charoula, T. Costas, T. Eleni, B. Anna, A. Elisavet, Hexavalent chromium removal from groundwater—A low-tech approach, Environ. Sci. Proceed 2 (1) (2020) 25.
[48] B. Fahimirad, A. Asghari, M. Rajabi, Magnetic graphitic carbon nitride nanoparticles covalently modified with an ethylenediamine for dispersive solid-phase extraction of lead (II) and cadmium (II) prior to their quantitation by FAAS, Microchim. Acta 184 (2017) 3027–3035.
[49] J. Sun, D. Meng, S. Jiang, G. Wu, S. Yan, J. Geng, Y. Huang, Multiple-bilayered RGO–porphyrin films: from preparation to application in photoelectrochemical cells, J. Mater. Chem. 22 (36) (2012) 18879–18886.
[50] Y. Chen, C. Zhang, X. Zhang, X. Ou, X. Zhang, One-step growth of organic single-crystal p–n nano-heterojunctions with enhanced visible-light photocatalytic activity, Chem. Commun. 49 (80) (2013) 9200–9202.
[51] P. Guo, P. Chen, M. Liu, One-dimensional porphyrin nanoassemblies assisted via graphene oxide: sheetlike functional surfactant and enhanced photocatalytic behaviors, ACS Appl. Mater. Interfaces 5 (11) (2013) 5336–5345.
[52] H. Kano, T. Kobayashi, Time-resolved fluorescence and absorption spectroscopies of porphyrin J-aggregates, J. Chem. Phys. 116 (1) (2002) 184–195.
[53] D. Zhou, C. Qiu, Study on the effect of Co doping concentration on optical properties of g-C3N4, Chem. Phys. Lett. 728 (2019) 70–73.
[54] Y. Li, S. Wu, L. Huang, J. Wang, H. Xu, H. Li, Synthesis of carbon-doped g-C3N4 composites with enhanced visible-light photocatalytic activity, Mater. Lett. 137 (2014) 281–284.
[55] M. Xu, L. Han, S. Dong, Facile fabrication of highly efficient g-C3N4/Ag2O heterostructured photocatalysts with enhanced visible-light photocatalytic activity, ACS Appl. Mater. Interfaces 5 (23) (2013) 12533–12540.
[56] D.D. La, S.V. Bhosale, L.A. Jones, N. Revaprasadu, S.V. Bhosale, Fabrication of a Graphene@ TiO2@ Porphyrin hybrid material and its photocatalytic properties under simulated sunlight irradiation, ChemistrySelect 2 (11) (2017) 3329–3333.
[57] J. Liu, T. Zhang, Z. Wang, G. Dawson, W. Chen, Simple pyrolysis of urea into graphitic carbon nitride with recyclable adsorption and photocatalytic activity, J. Mater. Chem. 21 (38) (2011) 14398–14401.
[58] B.V. Lotsch, M. Döblinger, J. Sehnert, L. Seyfarth, J. Senker, O. Oeckler, W. Schnick, Unmasking melon by a complementary approach employing electron diffraction, solid-state NMR spectroscopy, and theoretical calculations—structural characterization of a carbon nitride polymer, Chem. A Eur. J. 13 (17) (2007) 4969–4980.
[59] I. McConnell, G. Li, G.W. Brudvig, Energy conversion in natural and artificial photosynthesis, Chem. Biol. 17 (5) (2010) 434–447.
[60] J. Barber, Photosynthetic energy conversion: natural and artificial, Chem. Soc. Rev. 38 (1) (2009) 185–196.
[61] S. Mandal, S.K. Nayak, S. Mallampalli, A. Patra, Surfactant-assisted porphyrin based hierarchical nano/micro assemblies and their efficient photocatalytic behavior, ACS Appl. Mater. Interfaces 6 (1) (2014) 130–136.
[62] X. Liu, R. Ma, L. Zhuang, B. Hu, J. Chen, X. Liu, X. Wang, Recent developments of doped g-C3N4 photocatalysts for the degradation of organic pollutants, Crit. Rev. Environ. Sci. Technol. 51 (8) (2021) 751–790.
[63] J. Wen, J. Xie, X. Chen, X. Li, A review on g-C3N4-based photocatalysts, Appl. Surf. Sci. 391 (2017) 72–123.
[64] P.J. Meadows, E. Dujardin, S.R. Hall, S. Mann, Template-directed synthesis of silica-coated J-aggregate nanotapes, Chem. Commun. (29) (2005) 3688–3690.
[65] T. Muhmood, Z. Cai, S. Lin, J. Xiao, X. Hu, F. Ahmad, Graphene/graphitic carbon nitride decorated with AgBr to boost photoelectrochemical performance with enhanced catalytic ability, Nanotechnology 31 (50) (2020), 505602.
[66] T. Muhmood, M. Xia, W. Lei, F. Wang, M.A. Khan, Design of graphene nanoplatelet/graphitic carbon nitride heterojunctions by vacuum tube with enhanced photocatalytic and electrochemical response, Eur. J. Inorg. Chem. 2018 (16) (2018) 1726–1732.